Motivation and Design of a High Performance MHD Code

Darren De Zeeuw
University of Michigan

NASA Summer School
July 22, 2003

Outline

- Introduction
- Space weather phenomena
- Physics of Space Weather
- Physics Challenges for MHD
- Elements of an MHD Code
- BATSRUS

Key Participants and Collaborators

- Core development team at Michigan:
  - Application lead: Tamas Gombosi, Bob Clauer
  - Algorithm/Code development: Ken Powell, Darren De Zeeuw, Gábor Tóth, Igor Sokolov
  - Computer science/Software engineering: Quentin Stout, David Chesney, Bob Oehmke, Terry Weymouth,
  - Applications: K.C. Hansen, Chip Manchester, Aaron Ridley, Ilia Roussev
- Collaborators at Michigan:
  - Phil Roe, Bram van Leer
  - Len Fisk, Janet Kozyra, Mike Liemohn, Andy Nagy, Volodia Papitashvili, Nathan Schwadron, Thomas Zurbuchen
- Collaborators at other institutions:
  - Satnislav Sazykin, Dick Wolf (Rice)
  - Paulett Liewer, Merav Opher (JPL)
  - Tom Holzer, B.C. Low, Art Richmond, Ray Roble (NCAR)

Sponsors and Institutional Collaborations

- NSF
  - ATM Upper Atmosphere Division
  - Knowledge and Distributed Intelligence (KDI)
- NASA
  - Earth and Space Science HPCC Project (Grand Challenges, Round 2)
  - Computational Technologies Project (Grand Challenges, Round 3)
  - Space Science Enterprise AISRP
- DoD
  - Multidisciplinary University Research Initiative (MURI)
  - AFOSR
- CCMC (Community Coordinated Modeling Center)
  - BATSRUS is available for "runs on request"
  - Testing for space weather forecasting transitioning
- NOAA/SEC & AF/SpaceWOC
- Other partners
  - JPL
  - NCAR HAO
  - Rice University
  - University of Alberta
  - University of Arizona
  - University of New Hampshire
  - UCSD

Space Weather Phenomena

Center for Space Environment Modeling

http://csem.engin.umich.edu

Space Weather

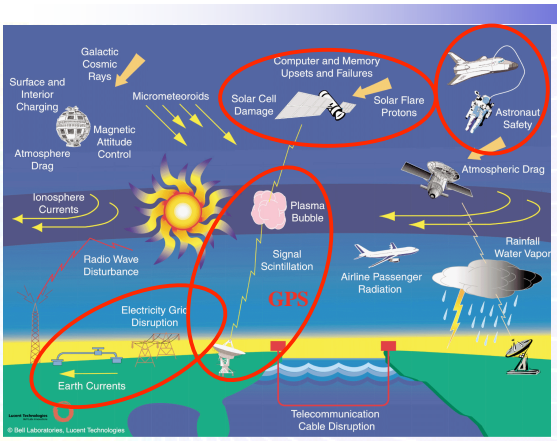

Conditions on the Sun and in the solar wind, magnetosphere, ionosphere, and thermosphere that can influence the performance and reliability of space-born and ground-based technological systems and can endanger human life or health.

Center for Space Environment Modeling

http://csem.engin.umich.edu

Solar Features & Space Weather

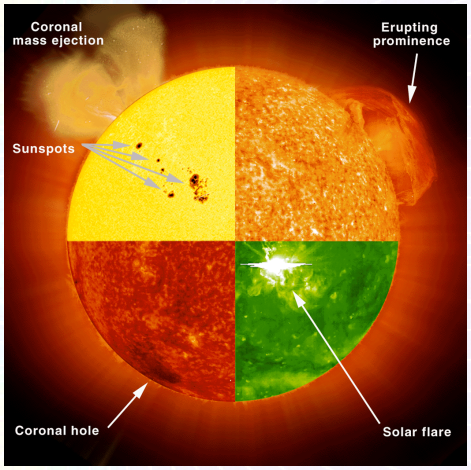

CME Series in April 2001 (SOHO LASCO C2)

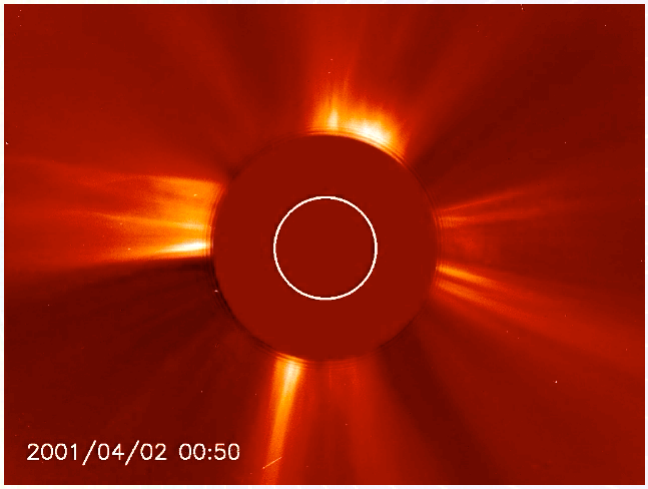

Geoeffectiveness

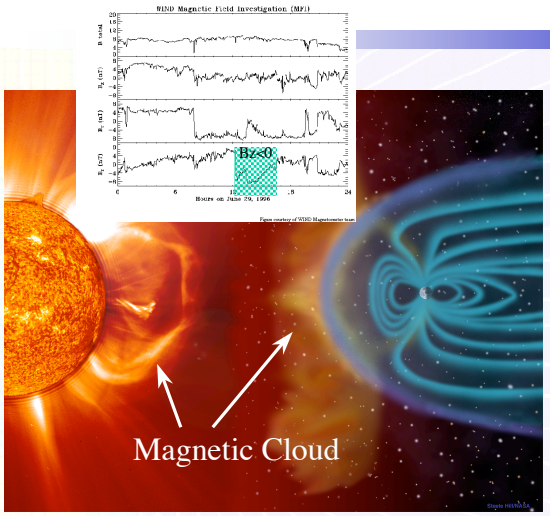

Sun to Earth in 3 Days

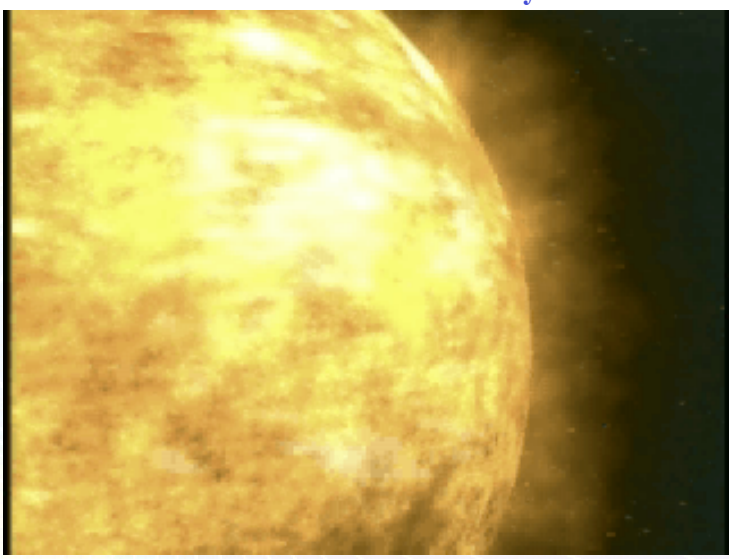

Aurora from Space

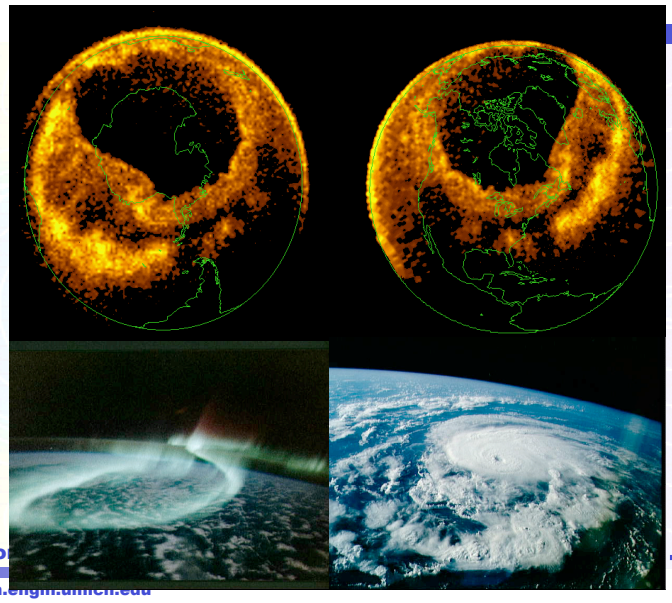

Center for

http://csem.engin.umich.edu

Space Weather and the Electric Power Grid

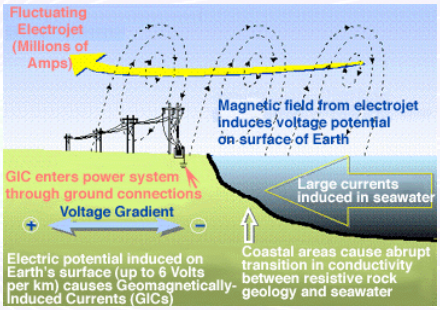

Space Weather and Transformers

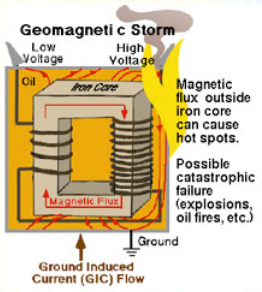

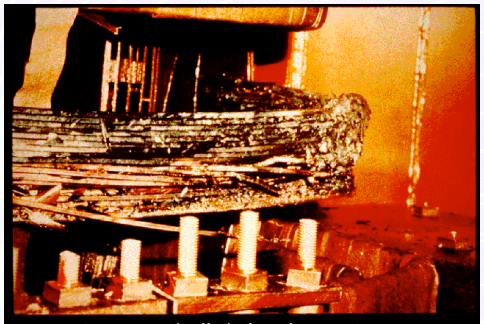

Geomagnetically induced currents from the flare events of March 1989 caused this $26 million transformer at the New Jersey PSC to meltdown

Physics of Space Weather

Magnetic Reconnection

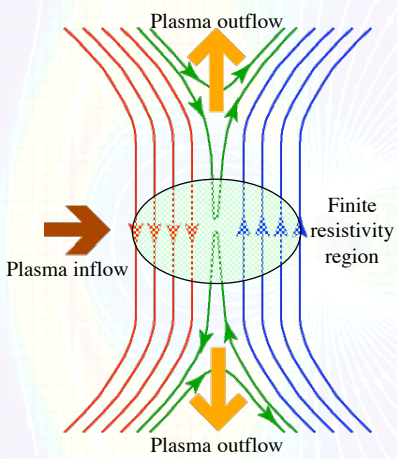

- In reconnection regions magnetic energy is converted to flow energy
- Reconnection rate only weakly depends on resistivity (~ log(□))
- Reconnected magnetic flux is controlled by the rate of flux transport into the reconnection region
- Magnetic reconnection is the major coupling mechanism between the solar wind and the magnetosphere

Center for Space Environment Modeling
http://csem.engin.umich.edu

Reconnection Movie

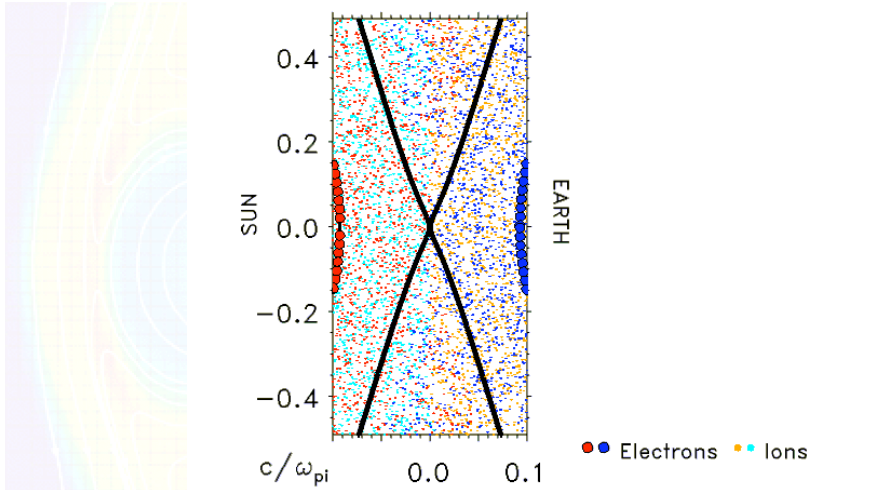

Magnetospheric Configurations

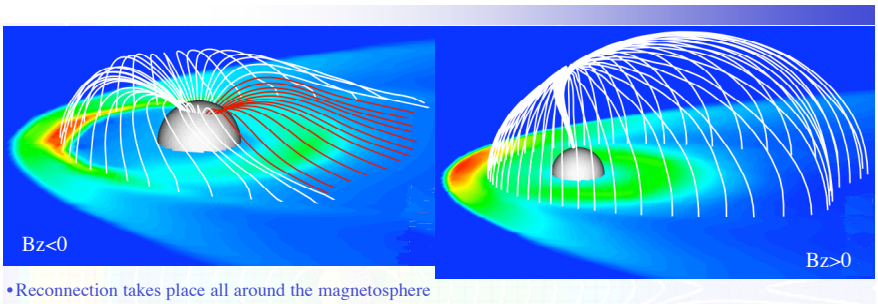

- Reconnection takes place all around the magnetosphere near the equatorial plane.
- White lines represent the last closed field lines just inside the magnetopause.
- Red lines represent the last closed field lines in the tail.
- Under equilibrium conditions the total magnetic flux reconnecting to Earth along the magnetopause is balanced by the magnetic flux disconnected in the tail.
- Magnetic reconnection is controlled by the magnetic flux transported by the solar wind to the magnetopause.

- Reconnection is limited to a very small region near the cusp.
- The magnetosphere is "closed" (however there is some disagreement).
- IMF field lines "attach" and "detach" at the cusp.
- Solar wind-magnetosphere plasma exchange is like "peeling an onion."
- Magnetospheric convection is quite complicated.

Physics Challenges for MHD

Simulating Space Weather

- Scales:
  - 1 Rs=109 Re
  - 1 AU=215 Rs =23,456 Re
  - Solar wind speed: 400-800 km/s ~ 4-8 Re/min
- Magnetosphere:
  - Subsolar bow shock distance: ~15 Re
  - Subsolar magnetopause distance: ~10 Re
  - Polar cap diameter: < 1 Re
  - Auroral oval thickness: <0.1 Re
  - Near Earth reconnection line distance (tail): ~25 Re
  - Distant reconnection line distance (tail): ~100 Re
- Space weather modeling is a truly multiscale challenge:
  - Simulation box size: ~50,000 Re^3
  - Simulation time: ~30 days
  - Smallest grid size: ~1/64 Re
  - Time resolution: ~1 min
- Presently the only viable method is magnetohydrodynamics (MHD) on solution adaptive grids (AMR MHD)

Center for Space Environment Modeling
http://csem.engin.umich.edu

MHD Equations

$$\frac{\partial \rho}{\partial t} + (\mathbf{u}\cdot\nabla)\rho + \rho(\nabla\cdot\mathbf{u}) = \dot{\rho} - L\rho$$

Electrodynamic coupling

$$\rho\frac{\partial \mathbf{u}}{\partial \mathbf{t}} + (\mathbf{u}\cdot\nabla)\mathbf{u} + \nabla p - \rho_e\mathbf{E} - \mathbf{j}\times\mathbf{B} = \rho\mathbf{g} + (\dot{\rho} + \hat{\eta}\rho)(\mathbf{u}_a - \mathbf{u})$$

$$\frac{3}{2}\frac{\partial p}{\partial t} + \frac{3}{2}(\mathbf{u}\cdot\nabla)p + \frac{5}{2}p(\nabla\cdot\mathbf{u}) = \dot{Q} + \frac{1}{2}(\dot{\rho} + \hat{\eta}\rho)(\mathbf{u}_a - \mathbf{u})^2 - \frac{3}{2}Lp$$

Semirelativistic MHD

$$\frac{\partial \mathbf{B}}{\partial \mathbf{t}} + \nabla\times\mathbf{E} = -\mathbf{u}(\nabla\cdot\mathbf{B})$$

$$\frac{1}{c^2}\frac{\partial \mathbf{E}}{\partial \mathbf{t}} - \nabla\times\mathbf{B} + \mu_0\mathbf{j}$$

$$\rho_e = \frac{1}{\mu_0 c^2}\nabla\cdot\mathbf{E}$$

$$\nabla\cdot\mathbf{B} = 0$$

Divergence B control

$$\mathbf{E} = -\mathbf{u}\times\mathbf{B} + \eta\mathbf{j}$$

Resistive MHD

Electromagnetic Coupling

- Weakly coupled formulation
  - Hydrodynamic quantities in conservative form, electrodynamic terms in source term
  - Hydrodynamic conservation & jump conditions
  - One characteristic wave speed (ion-acoustic)

$$\frac{\partial}{\partial t}\begin{bmatrix}\rho \\ \rho\mathbf{u} \\ \frac{1}{2}\rho u^2 + \frac{1}{\gamma-1}p\end{bmatrix} + \nabla\cdot\begin{bmatrix}\rho\mathbf{u} \\ \rho\mathbf{u}\mathbf{u} + \mathbf{I}p \\ \left[\frac{1}{2}\rho u^2 + \frac{\gamma}{\gamma-1}p\right]\mathbf{u}\end{bmatrix}^T = \begin{bmatrix}0 \\ \frac{1}{\mu_0}\mathbf{j}\times\mathbf{B} \\ 0\end{bmatrix}^T$$

$$\frac{\partial \mathbf{B}}{\partial \mathbf{t}} = \nabla\times(\mathbf{u}\times\mathbf{B})$$

$$\mathbf{j} = \frac{1}{\mu_0}\nabla\times\mathbf{B}$$

- Tightly coupled formulation
  - Fully conservative form
  - MHD conservation and jump conditions
  - Three characteristic wave speeds (slow, Alfvén, fast)
  - One degenerate eigenvalue/eigenvector

$$\frac{\partial}{\partial t}\begin{bmatrix}\rho \\ \rho\mathbf{u} \\ \frac{1}{2}\rho u^2 + \frac{1}{\gamma-1}p + \frac{1}{2\mu_0}B^2 \\ \mathbf{B}\end{bmatrix} + \nabla\cdot\begin{bmatrix}\rho\mathbf{u} \\ \rho\mathbf{u}\mathbf{u} + \left(p + \frac{1}{2\mu_0}B^2\right)\mathbf{I} - \frac{1}{\mu_0}\mathbf{B}\mathbf{B} \\ \left[\frac{1}{2}\rho u^2 + \frac{\gamma}{\gamma-1}p + \frac{1}{2\mu_0}B^2\right]\mathbf{u} - \frac{1}{\mu_0}(\mathbf{u}\cdot\mathbf{B})\mathbf{B} \\ \mathbf{u}\mathbf{B} - \mathbf{B}\mathbf{u}\end{bmatrix}^T = \begin{bmatrix}0 \\ 0 \\ 0 \\ 0\end{bmatrix}^T$$

Brio-Wu Problem

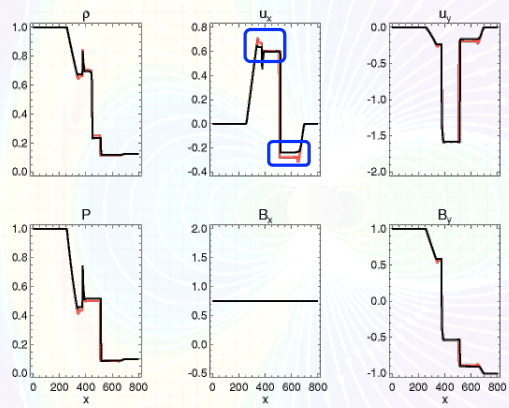

- Tightly coupled formulation (Balsara & Spicer 1999)
  - Ensures MHD jump conditions
  - All jumps are correct
- Weakly coupled formulation (Evans & Hawley 1988)
  - Ensures HD jump conditions
  - Small errors in density and pressure
  - ~20% error in normal velocity component

Symmetrizability

- Faraday's law does not "know" that no magnetic monopoles were ever found in our universe:

$$\frac{\partial \mathbf{B}}{\partial t} + \nabla \times \mathbf{E} = \nabla \mathbf{u}(\nabla \cdot \mathbf{B})$$

- Symmetrizable system:

$$\frac{\partial \mathbf{U}}{\partial t} + \mathbf{A}_x \frac{\partial \mathbf{U}}{\partial x} + \mathbf{A}_y \frac{\partial \mathbf{U}}{\partial y} + \mathbf{A}_z \frac{\partial \mathbf{U}}{\partial z} = 0$$

  where $\mathbf{A}_x$, $\mathbf{A}_y$, and $\mathbf{A}_z$ are symmetrizable matrices.
  - Symmetrizable systems, and only symmetrizable systems, are formally Galilean invariant.
  - Symmetrizable systems admit an additional conservation law for an entropy function.
  - Conversely, one can always construct a symmetrizable system of conservation laws from the entropy function.
- Symmetriazability of ideal MHD (Godunov 1972)
  - The ideal MHD equations without the $\nabla \cdot \mathbf{B}$ term in Faraday's law are not symmetrizable.
  - The MHD system becomes symmetrizable only by keeping the $\nabla \cdot \mathbf{B}$ terms in Faraday's law.
  - The symmetrizable MHD system has 8 non-degenerate eigenvalues/eigenvectors.
  - For MHD (and for the Euler equations) the entropy function is $S=p/\rho^{\gamma}$.

Symmetrizable MHD Equations

- The symmetrizable MHD equations can be written in a near-conservative form:

$$\frac{\partial}{\partial t}\begin{bmatrix}\rho \\ \rho\mathbf{u} \\ \frac{1}{2}\rho u^2 + \frac{1}{\rho(\gamma-1)}p + \frac{1}{2\mu_0}B^2 \\ \mathbf{B}\end{bmatrix} + \nabla\cdot\begin{bmatrix}\rho\mathbf{u} \\ \rho\mathbf{u}\mathbf{u} + \left(p + \frac{1}{2\mu_0}B^2\right)\mathbf{I} - \frac{1}{\mu_0}\mathbf{B}\mathbf{B} \\ \left[\frac{1}{2}\rho u^2 + \frac{\gamma}{\rho(\gamma-1)}p + \frac{1}{2\mu_0}B^2\right]\mathbf{u} - \frac{1}{\mu_0}(\mathbf{u}\cdot\mathbf{B})\mathbf{B} \\ \mathbf{u}\mathbf{B} - \mathbf{B}\mathbf{u}\end{bmatrix}^T = -(\nabla\cdot\mathbf{B})\begin{bmatrix}0 \\ \frac{1}{\mu_0}\mathbf{B} \\ \frac{1}{\mu_0}(\mathbf{u}\cdot\mathbf{B}) \\ \mathbf{u}\end{bmatrix}$$

- Deviation from total conservative form is of the order of $\nabla\cdot\mathbf{B}$ truncation errors
- $\nabla\cdot\mathbf{B}$ truncation errors are advected (they do not "stick" to the grid), because

$$\frac{\partial(\nabla\cdot\mathbf{B})}{\partial t} + \underbrace{\nabla\cdot(\nabla\times\mathbf{E})}_{0} + \nabla\cdot\left[\mathbf{u}(\nabla\cdot\mathbf{B})\right] = 0$$

- The symmetrizable MHD equations lead to the 8-wave method of $\nabla\cdot\mathbf{B}$ control
  - Robust and accurate
  - Consistent with modern finite volume shock capturing methods

Semi-Relativistic MHD: Motivation

- The Alfvén speed can approach or exceed the speed of light in many space physics problems (auroral zones, near the Sun, etc.). $V_A > c$ is clearly unphysical, so one needs to restrict the Alfvén speed.
- A large Alfvén speed also poses a severe problem for numerical modeling:
  - The time steps of an explicit time integration scheme are limited by the Courant-Friedrichs-Lewy (CFL) numerical stability condition: the waves must not propagate more than one cell size in one time step.
  - In a well resolved simulation, the smallest cell size may be ≤100 km, which limits the time step to be less than 0.01 or even 0.001 seconds. On the other hand, typical time-scales of the magnetosphere are on the order of minutes to hours.
- Semi-relativistic MHD:
  - Electrodynamics is treated in a fully relativistic manner (keep the displacement current).
  - All particle speeds (bulk and thermal) are non-relativistic.

Semi-Relativistic MHD

- **Non-relativistic Alfvén speed:**

$$V_A = \frac{B}{\sqrt{\mu_0 \rho}}$$

- **Alfvén speed** in some solar system plasmas:

Region	V_A/c
Earth's auroral zone	~ 0.1
Saturn's polar region	~ 1
Jupiter's polar region	~ 10

Be careful with non-relativistic MHD when modeling planets with strong intrinsic magnetic field!

- **Solution:**
  - All particle speeds are non-relativistic (u and a_s),
  - Alfvén speed can be relativistic.
- **Ampère's law** for ideal MHD

$$\mu_0 \mathbf{j} = \nabla \times \mathbf{B} + \frac{1}{c^2}\frac{\partial}{\partial t}(\mathbf{u} \times \mathbf{B})$$

What Changes Relativity Makes

- Semi-relativistic MHD combines the non-relativistic fluid equations with relativistic electrodynamics. The governing equations are now derived by keeping the displacement current in Ampère's law. In this case the normalized state vector and flux diad become the following:

$$\mathbf{W} = \left[\rho, \rho\mathbf{u} + \tfrac{1}{c^2}(\mathbf{E} \times \mathbf{B}), \mathbf{B}, \tfrac{1}{2}\rho u^2 + \tfrac{p}{\gamma - 1} + \tfrac{1}{2}\left(B^2 + \tfrac{1}{c^2}E^2\right)\right]^{\mathsf{T}}$$

$$\mathbf{F} = \begin{bmatrix} \rho\mathbf{u} \\ \rho\mathbf{u}\mathbf{u} + \left(p + \frac{1}{2}B^2 + \frac{1}{2c^2}E^2\right)\mathbf{I} - \mathbf{B}\mathbf{B} - \frac{1}{c^2}\mathbf{E}\mathbf{E} \\ \mathbf{u}\mathbf{B} - \mathbf{B}\mathbf{u} \\ \mathbf{u}\left(\frac{1}{2}\rho u^2 + \frac{p}{\gamma - 1} + p\right) + \mathbf{E} \times \mathbf{B} \end{bmatrix}^{\mathsf{T}}$$

where

$$\mathbf{E} = -\mathbf{u} \times \mathbf{B}$$

- **Wave speeds:**

$$\lim_{V_A^2 \to \infty} c_s^* = a \qquad \lim_{V_A^2 \to \infty} V_A^* = c \qquad \lim_{V_A^2 \to \infty} c_f^* = c$$

Elements of an MHD Code

Upwind Differencing

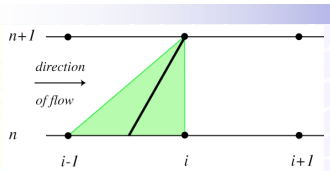

- The "one-way wave equation" propagating to the right:

$$\frac{\partial \phi}{\partial t} + a\frac{\partial \phi}{\partial x} = 0 \qquad a > 0$$

- When the wave equation is discretized "upwind" (i.e. using data at the old time level that comes from the left the wave equations becomes:

$$\phi_i^{n+1} = \phi_i^n + \frac{a\Delta t}{\Delta x}\left(\phi_{i-1}^n - \phi_i^n\right) = (1-\alpha)\phi_i^n + \alpha\phi_{i-1}^n \qquad \alpha \le 1$$

- Advantages:
  - Physical: The numerical scheme "knows" where the information is coming from
  - Robustness: The new value is a linear interpolation between two old values and therefore no new extrema are introduced

Finite Volume Method

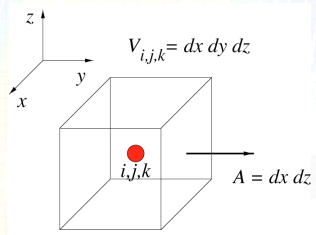

Computational Cell

- Conservative (divergence) form of conservation laws:

$$\frac{dU}{dt} + \nabla \cdot F = S$$

- Volume integral for computational cell:

$$\frac{dU_{i,j,k}}{dt} = -\sum_{faces} A \cdot F + S_{i,j,k}$$

- Fluxes of mass, momentum, energy and magnetic field entering from one cell to another through cell interfaces are the essence of finite volume schemes. This is a Riemann problem.

Riemann Solver

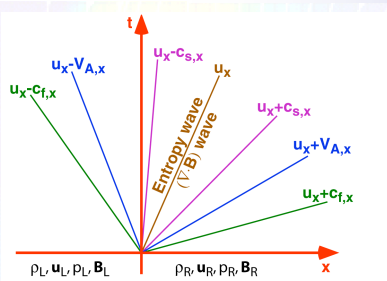

- Discontinuous initial condition
  - Interaction between two states
  - Transport of mass, momentum, energy and magnetic flux through the interface due to waves propagating in the two media
- Riemann solver calculates interface fluxes from left and right states

- At the interface consider 1D advection:

$$\frac{\partial \mathbf{U}}{\partial t} + \frac{\partial \mathbf{F}}{\partial x} = 0$$

- The eigenvalues and eigenvectors of the Jacobian, $\partial\mathbf{F}/\partial\mathbf{U}$ are at the heart of the Riemann solver:

$$\mathbf{F}_{LR} = \frac{1}{2}(\mathbf{F}_L + \mathbf{F}_R) - \frac{1}{2}\sum_{k=1}^{8} R_k |\lambda_k| L_k (\mathbf{U}_R - \mathbf{U}_L)$$

  - Each wave is treated in an upwind manner
  - The interface flux function is constructed from the individual upwind waves
  - For each wave the artificial dissipation (necessary for stability) is proportional to the corresponding wave speed

Limited Linear Reconstruction

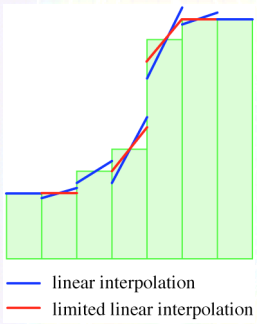

- Finite volume data is stored at the cell centers, while fluxes need to be computed at the interfaces between cells (faces). Thus, we need an interpolation scheme to give accurate values at the two sides of the interface.
- Reconstruction process can introduce new extrema. We need to limit the slopes so that the reconstructed values are bounded by the values used to create the reconstruction.
- Limited reconstruction:

$$W_k(x) = W_k(x_c) + \Phi_k W_k \cdot (x - x_c)$$

- Near discontinuities $\Phi = 0$ (first-order scheme), in smooth regions $\Phi = 1$ (second-order scheme).

The divB=0 Problem

- $\nabla \cdot \mathbf{B}$ in nature:
  - $\nabla \cdot \mathbf{B} = 0$ is an observation (people are still searching for magnetic monopoles…)
- Conservation of $\nabla \cdot \mathbf{B} = 0$:
  - Analytically: if $\nabla \cdot \mathbf{B} = 0$ at t=0 than it remains zero at all times
  - Numerically: In shock capturing schemes the curl and div operators do not commute
- Approaches:
  - Purist: Maxwell's equations demand $\nabla \cdot \mathbf{B} = 0$ exactly, so $\nabla \cdot \mathbf{B}$ must be zero numerically
  - Modeler: There is truncation error in components of B, so what is special in a particular discretized form of $\nabla \cdot \mathbf{B}$?
- Purposes to control $\nabla \cdot \mathbf{B}$ numerically:
  - To improve accuracy
  - To improve robustness
  - To avoid unphysical effects (like parallel Lorentz force)
  - To make purists happy

$\nabla\cdot\mathbf{B}$ Control Methods in a Nutshell

- Projection scheme (Barnes & Brackbill 1980)
  - Update **B** with base scheme
  - Solve Poisson equation $\nabla\cdot\mathbf{B} = \nabla^2\phi$
  - Obtain divergence free magnetic field, $\mathbf{B}^* = \mathbf{B} - \nabla\phi$
- Constrained transport scheme (Evans & Hawley 1988, Dai & Woodward 1998, Balsara & Spicer 1999)
  - Interpolate fluxes of the base scheme to edge center and update electric field
  - Update staggered normal magnetic field components at face center with $\nabla\times\mathbf{E}$
  - Conserve $\nabla\cdot\mathbf{B}=0$ to machine accuracy for staggered discretization
- 8-wave scheme (Powell 1994)
  - Re-derive MHD equations with keeping the $\nabla\cdot\mathbf{B}$ term
  - Discretize this form to achieve symmetrizability and formal Galilean invariance
  - This allows truncation level errors in $\nabla\cdot\mathbf{B}$, but advects it
- Diffusive control (Marder 1987, Dedner et al., 2001)
  - Add terms to 8-wave scheme that diffuse $\nabla\cdot\mathbf{B}$
  - This reduces $\nabla\cdot\mathbf{B}$ errors by an order of magnitude

Comparison of $\nabla\cdot\mathbf{B}$ Control Methods (IMF North, 370,000 cells, 0.25–8 R_E cell size)

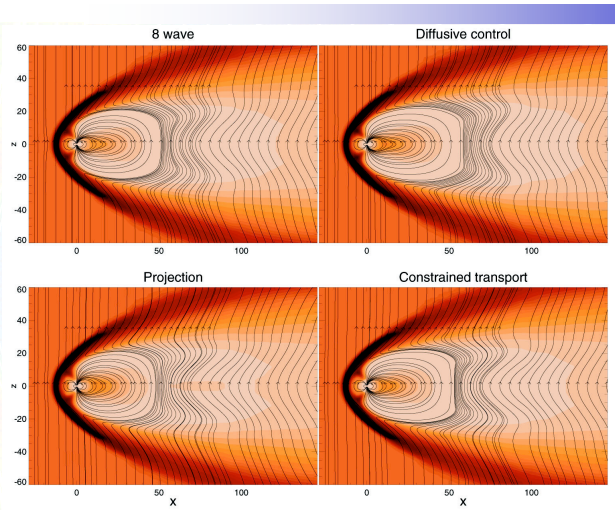

Time-Stepping

- Two-stage, second-order explicit time stepping (predictor-corrector)
  - Highly localized and well suited for parallel machines
  - Time step is limited by the fastest local wave (~10^{-2} s for magnetosphere)
- Local time-stepping for steady-state solutions (not sub-cycling)
  - Use time-step permitted by the local CFL condition in very cell
  - $\mathbf{U}_i^{n+1} = \mathbf{U}_i^n + \Delta t_i[\nabla(\nabla \cdot \mathbf{F})_i^n + \mathbf{S}_i^n]$; in steady-state $\Delta t_i[\nabla(\nabla \cdot \mathbf{F})_i^n + \mathbf{S}_i^n]=0$
  - About 20 times faster than time-accurate calculation
- Boris correction
  - Use semi-relativistic MHD and artificially lower c by about a factor of 100
  - Results in ~10 speedup
- Implicit time-stepping
  - First-order in time backward Euler scheme for steady state
  - Second-order in time BDF2 scheme for time-accurate simulations
  - Newton iteration to solve non-linear equation
  - Krylov-type iterative solver to solve the linear systems
  - Schwarz-type preconditioner to accelerate convergence

Time-Stepping Comparison

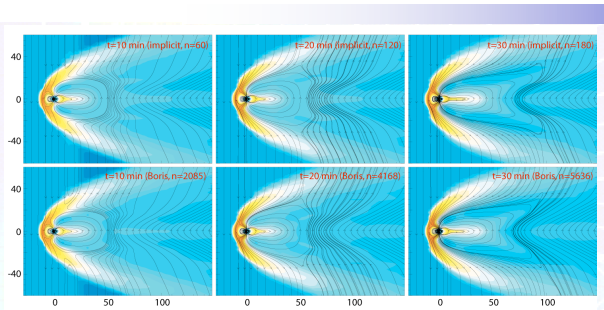

- IMF North to South turning
- 285,000 cells
- 0.25 - 8 R_E cell size
- Results shown in noon-midnight plane
- 16 PE Beowulf cluster w. 800MHz Athlon processors

Scheme	Time step (s)	CPU time/Time step	Real time/CPU time
Explicit	0.011	2.08	0.5%
Explicit (Boris c/200)	0.284	2.87	9.9%
Implicit	2.000	31.63	6.3%
Implicit	10.000	46.54	21.5%
Explicit/Implicit	2.000	8.94	22.4%

BATSRUS

BATSRUS:
Block Adaptive Tree Solar-wind Roe-type Upwind Scheme

- Physics
  - Semi-relativistic MHD
  - Four $\nabla \cdot \mathbf{B}$ control methods (8 wave, projection, diffusion, constrained transport)
  - Conservative, tightly coupled formulation
- Finite volume scheme
- High-resolution upwind scheme
  - Upwind differencing
  - Limited linear reconstruction
  - Approximate Riemann solver (Roe, Rusanov/Lax-Friedrichs, Linde, Artificial wind)
- Explicit, implicit and explicit/implicit time-stepping
- AMR & data structure
  - Adaptive self-similar blocks
  - Octree data structure
- Parallel implementation
  - Fortran-90 with MPI implementation
  - Near-perfect parallel scaling to >1500 PEs

Center for Space Environment Modeling
http://csem.engin.umich.edu

AMR & Data Structure

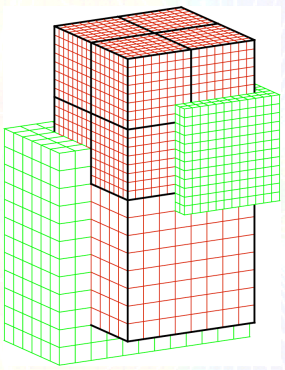

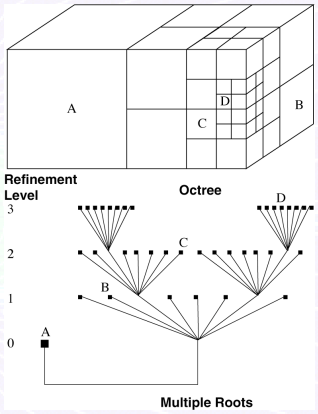

Dynamic Grid Refinement

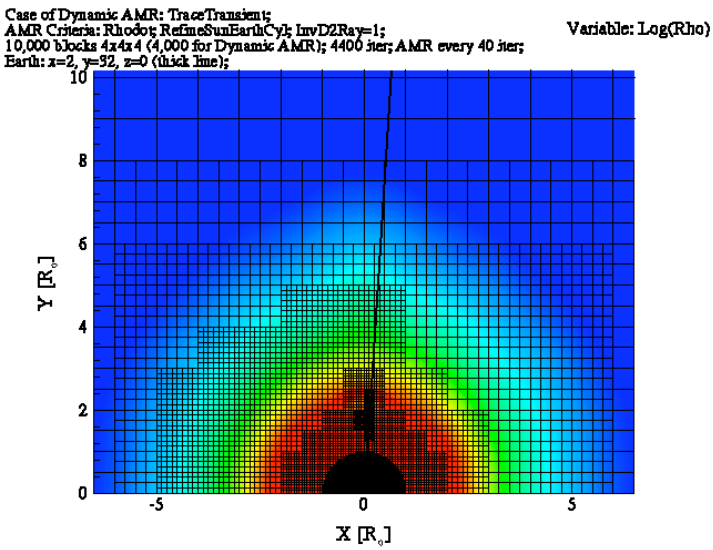

Distributing the Work to Processors

- No Load Balancing
- Processors get blocks based on refinement level
  - Red: 52 blocks
  - Green: 158 blocks
  - Blue: 20 blocks

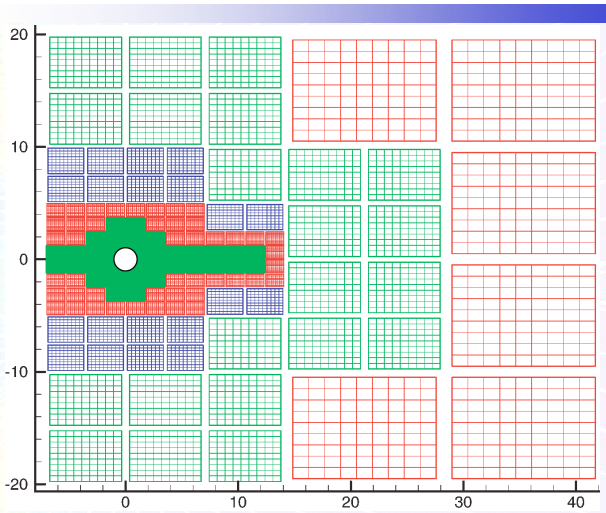

Distributing the Work to Processors

- Simple Load Balancing
- Processors get same number of blocks, but not attempt to cluster them
  - Red: 77 blocks
  - Green: 77 blocks
  - Blue: 76 blocks

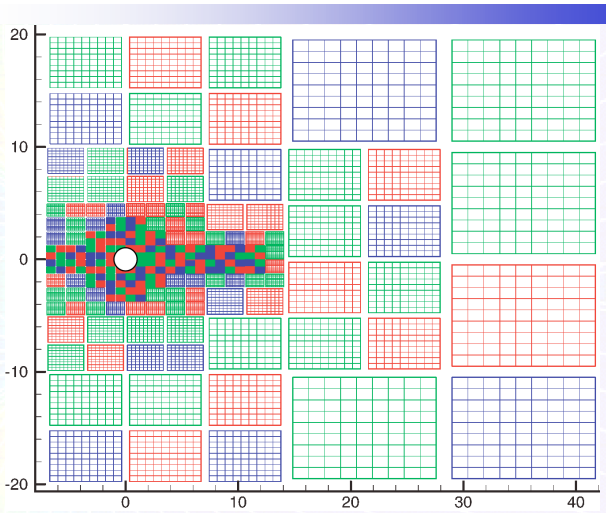

Distributing the Work to Processors

- Better Load Balancing
- Processors get same number of blocks, but now they are clustered together
  - Red: 77 blocks
  - Green: 77 blocks
  - Blue: 76 blocks

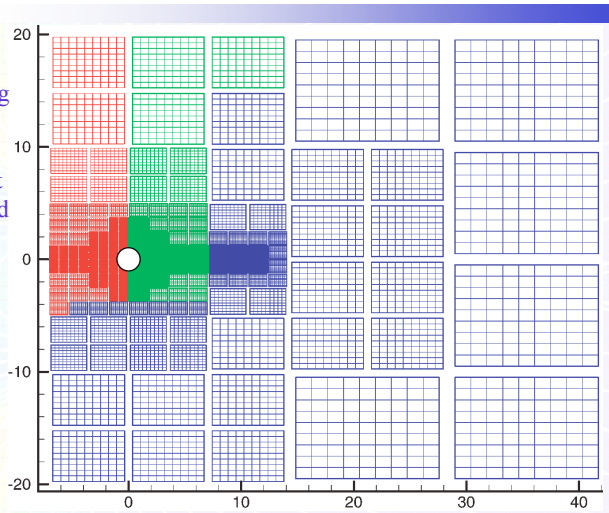

Parallel Implementation and Scaling

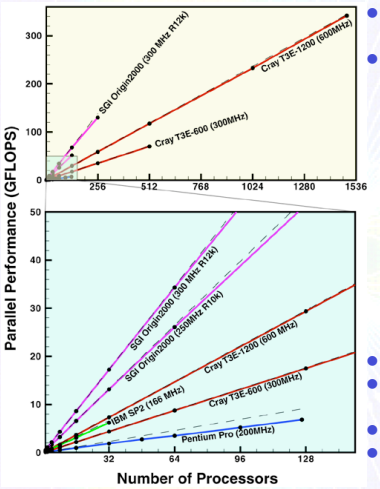

- Domain decomposition with self-similar adaptive blocks
- Peano-Hilbert space filling curve is used to minimize inter-processor communication

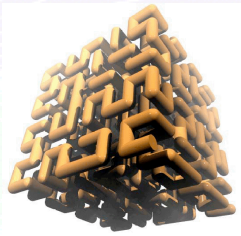

- Code is written in Fortran-90 with MPI
- Fully portable to Cray T3E/T3D, SGI Origin-2000/3000, IBM SP2/SP3, Linux cluster (Beowulf)
- Near-perfect scaling up to at least 1,500 processors
- Sustained performance of 345 Gflops on a Cray T3E-1200

Building a Parallel Implicit Solver

- Explicit schemes have dt limited by CFL condition: dt < dx/fastest wave speed
- High Alfvén speeds and/or small cells may lead to smaller time steps than desired
- The problem is particularly acute near planets with strong magnetic fields
- Implicit schemes do not have dt limited by CFL

- Second-order implicit time-stepping scheme requires solution of a large nonlinear system of equations at each time step
- Newton linearization allows the nonlinear system to be solved by an iterative process in which a large linear system is solved
- Krylov technique (GMRES) is a robust and efficient way to solve a large linear system
- Schwarz preconditioner (Modified block ILU) allows the process to be done in parallel
  - Each adaptive block solves the linear system corresponding to its local data
  - Blocks pass necessary information to neighboring blocks

Timing Results

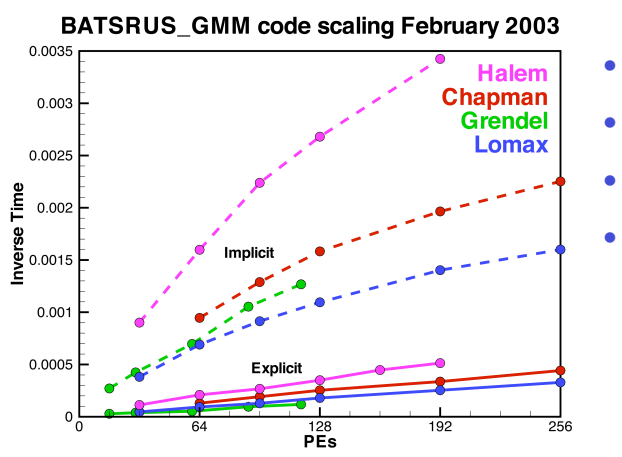

- Halem = 192 CPU Compaq ES-45
- Chapman = 256 CPU SGI 3800
- Lomax = 256 CPU Compaq ES-45
- Grendel = 120 CPU PC Cluster (1.6 GHz AMD)

Getting the Best of Both Worlds - Partial Implicit

- Fully implicit scheme has no CFL limit, but each iteration is expensive (memory and CPU)
- Fully explicit is inexpensive for one iteration, but CFL limit may mean a very small dt
- Block structure allows a partial implicit scheme
  - Solve blocks with unrestrictive CFL explicitly
  - Solve blocks with restrictive CFL implicitly
  - Modify block distribution for load balancing

Timing Results for Space Weather on Compaq

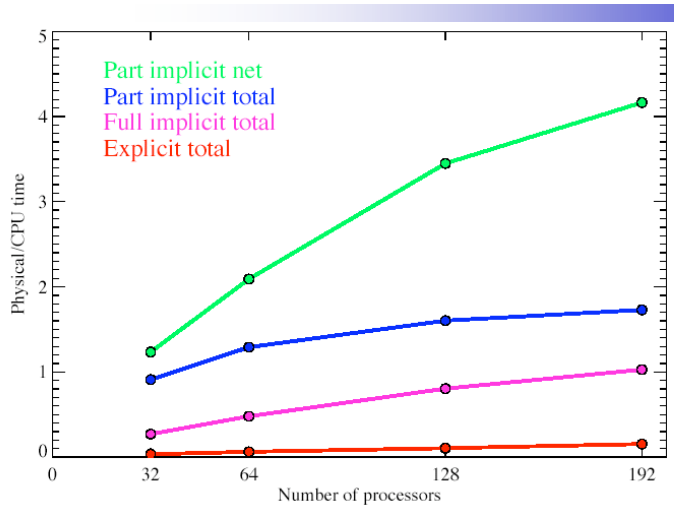

Code Validation

- Are the equations being solved correctly?
  - Basic symmetries are preserved
  - Comparison with exact solutions to PDEs
    - Smooth
    - Discontinuous
  - Comparison with highly resolved problems for which exact solutions are not known (grid convergence)
    - "Classic" test cases (shock tubes, Brio-Wu problem, Orszag-Tang vortex, etc.)
    - Controlled physically relevant problems (idealized magnetosphere for northward IMF)
- Are the equations being solved the correct description of physics?
  - Statistical validation (can the code capture empirically observed trends?)
  - Dynamic validation (event studies)

Grid Convergence

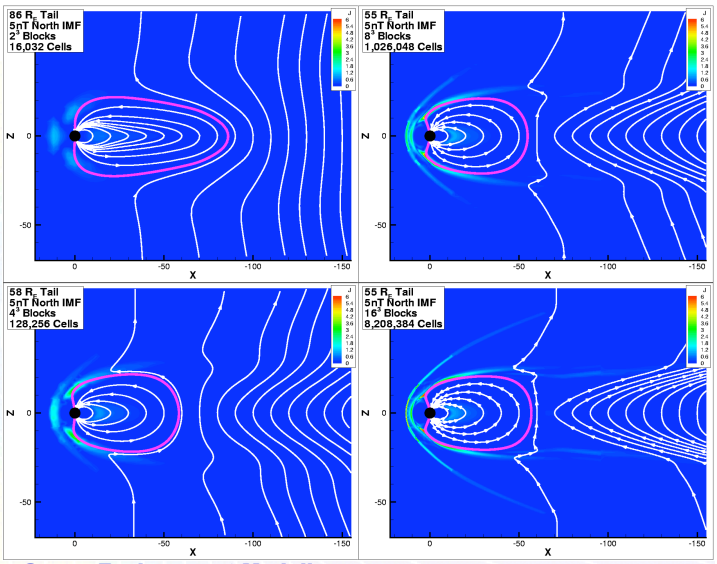

Event Study: GGCM Metrics Challenge

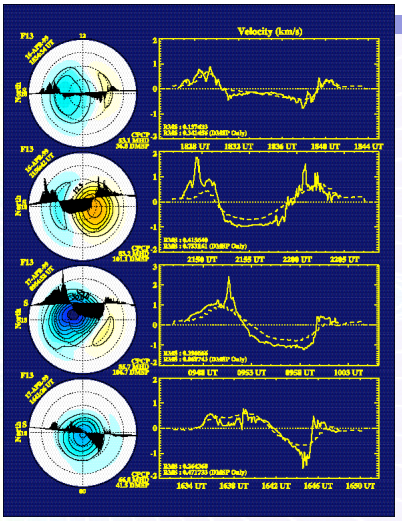

Summary

Center for Space Environment Modeling

http://csem.engin.umich.edu

Plans for the Future

- Framework development
  - Code coupling
  - Code speedup
  - "plug-and-play"
- Transition to space weather forecasting
  - Work with CCMC, NOAA/SEC and AF/SpaceWOG
- Community tool development
  - Work with space physics community
  - Web based access
- Physics investigations
  - Magnetic storms
  - CME initiation and propagation
  - SEP, radiation belt, plasmasphere
  - Event studies
- Improve physics
  - Resistive MHD
  - Heat conduction
- True multispecies MHD
  - Ionospheric outflow
  - Jupiter and Saturn

Applications of BATSRUS to Space Plasmas

Darren De Zeeuw
University of Michigan

NASA Summer School
July 22, 2003

Space Weather Related Applications

- 3D simulation of the inner heliosphere
  - Solar wind acceleration by energy deposition
  - Open/closed magnetic field lines
  - Two-state solar wind (solar minimum conditions)
  - Simulation extends from 1 Rs to 1 AU
- Solar eruptive event simulations
  - Localized density pulse driven eruption
  - Sheered arcade generated eruption (2D and 3D)
  - Self-similar erupting flux rope (reproduce the (Gibson & Low, 1998) solution)
  - Gibson-Low (1998) erupting flux rope initiates a CME in a “quite-time” solar wind
- Magnetosphere configurations
  - Steady-state simulations of “basic” magnetospheric topologies (IMF N, S, By only)
  - Use steady-state simulations for short dynamic periods (electrojet challenge)
- Event studies
  - Synthetic events with controlled input (pressure pulse, IMF turning)
  - Real events (GGCM metrics challenge, Bastille Day event)

Center for Space Environment Modeling
http://csem.engin.umich.edu

Solar System Simulations

- Solar wind interaction with terrestrial planets
  - Mercury
  - Venus
  - Mars
- Magnetospheres of Jupiter and Saturn
  - Jupiter during the Cassini flyby
  - Planetary satellites (Io, Europa, Titan)
  - Simulation of the Saturn-Titan two-body system
- Comets
  - Solar wind interaction with comets (Halley, Hyakutake, Hale-Bopp, Wirtanen,Borelli)
  - Origin of cometary x-ray emission (Hyakutake, Hale-Bopp)
- Heliosphere interaction with the local interstellar medium
  - Outer heliosphere
  - Interstellar pickup ions and the hydrogen wall

Adaptive Physics Domain Approach

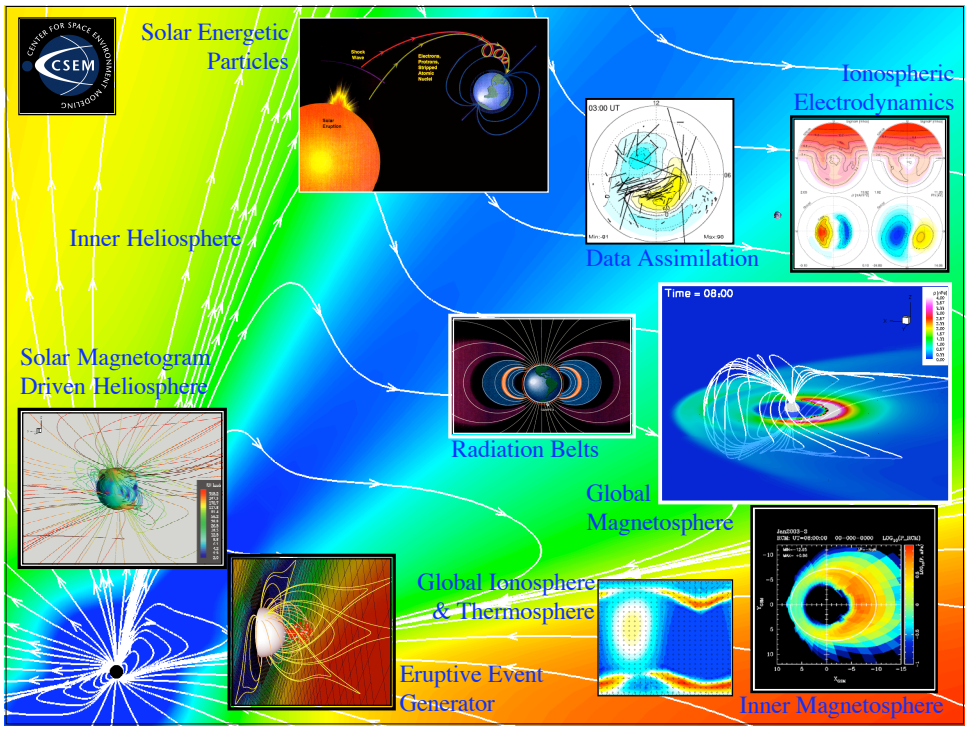
Solar Energetic Particles
Ionospheric Electrodynamics
Inner Heliosphere
Data Assimilation
Solar Magnetogram Driven Heliosphere
Radiation Belts
Global Magnetosphere
Global Ionosphere & Thermosphere
Eruptive Event Generator
Inner Magnetosphere

"Sun-to-Mud" Simulation
Center for Space Environment Modeling
http://csem.engin.umich.edu

Sun-to-Earth Simulation

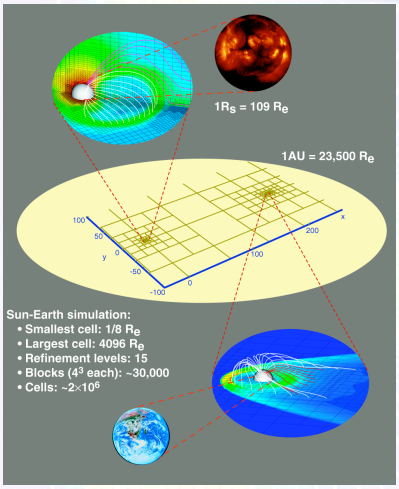

- A 3D "quiet-time" solar wind is generated that reproduces the basic properties of the inner heliosphere (1 Rs to ~1 AU).
- A localized density pulse initiates a solar eruptive event.
- The evolution and outward propagation of the interplanetary transient is simulated with frequent AMR
  - Simulation uses 1 to 2 million cells
  - Simulation was faster than real time on a Cray T3E-600 with 512 processors
- The interaction of the transient with the magnetosphere-ionosphere system was simulated

Quiet-Time 3D Solar Wind

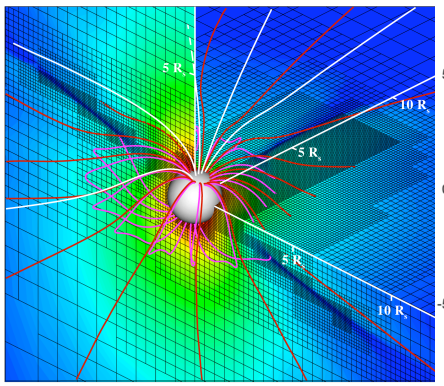

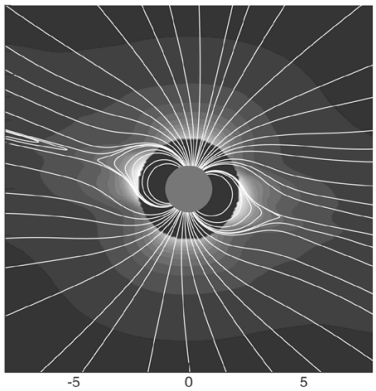

Density-Pulse Driven CME

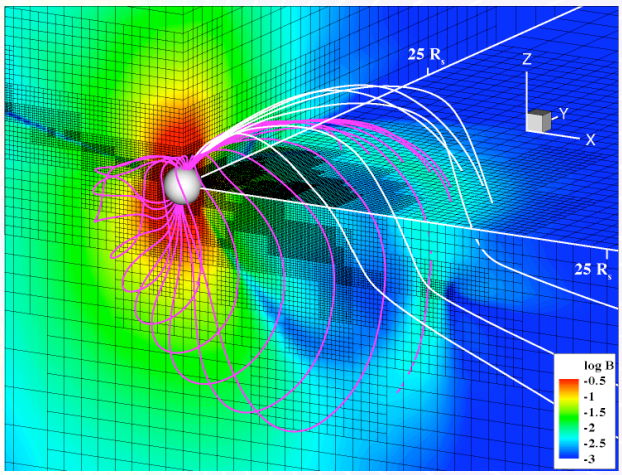

Interaction with the Magnetosphere-Ionosphere System

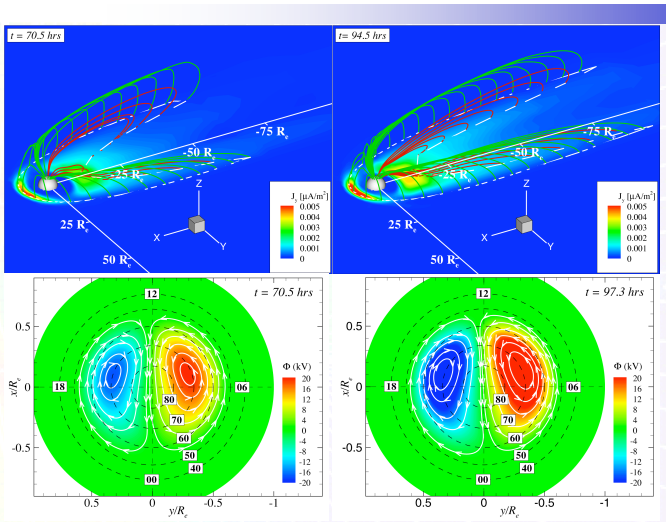

Coronal Flux Rope Eruption

Self-Similar Flux Rope Eruption

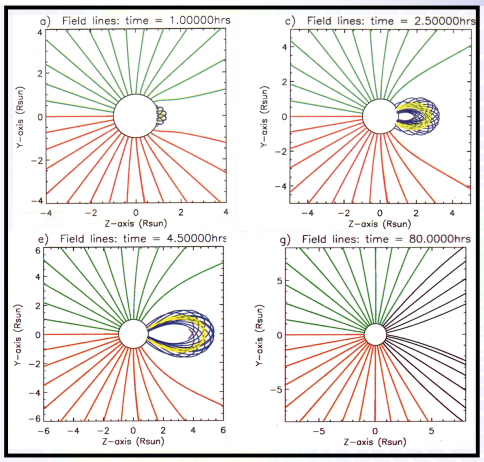

Gibson & Low, 1998

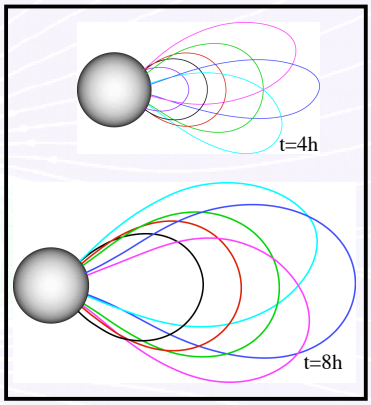

Numerical solution

Center for Space Environment Modeling
http://csem.engin.umich.edu

CME Generation by Flux-Rope Eruption

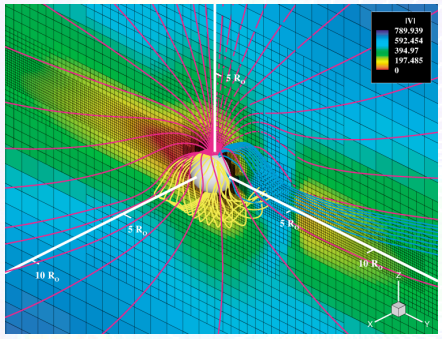

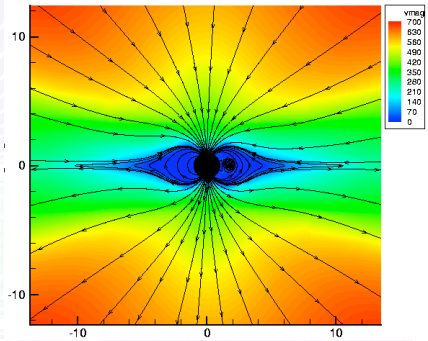

At t=0 the Gibson-Low (1998) analytic expression for an erupting flux rope is superimposed on a 3D quiet solar wind solution. The flux eruption and its interaction with the background solar wind is calculated with BATSRUS.

3D View of the Flux Rope in the Corona

- Magnetic field lines are drawn as solid colored lines at t= 0 hours.
- The flux rope is drawn with blue and red lines while orange and yellow lines show the poloidal field of the steady-state equatorial streamer belt.
- On the x-z plane, the computational mesh is drawn with black lines superimposed upon a false color image of the velocity magnitude.

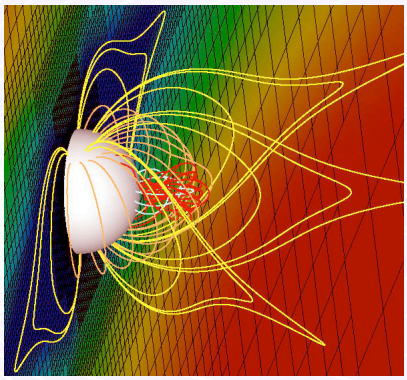

Properties of the Initial State

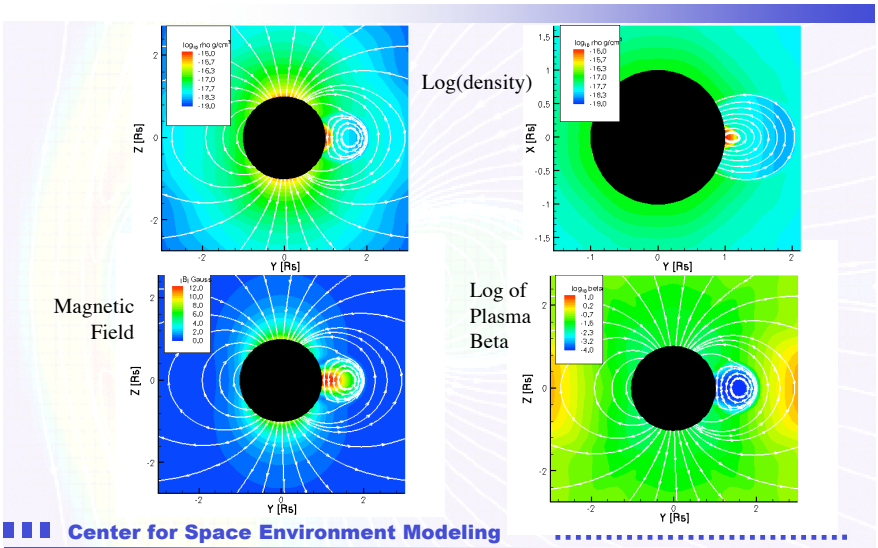

3D View of Velocity and Magnetic Field Lines

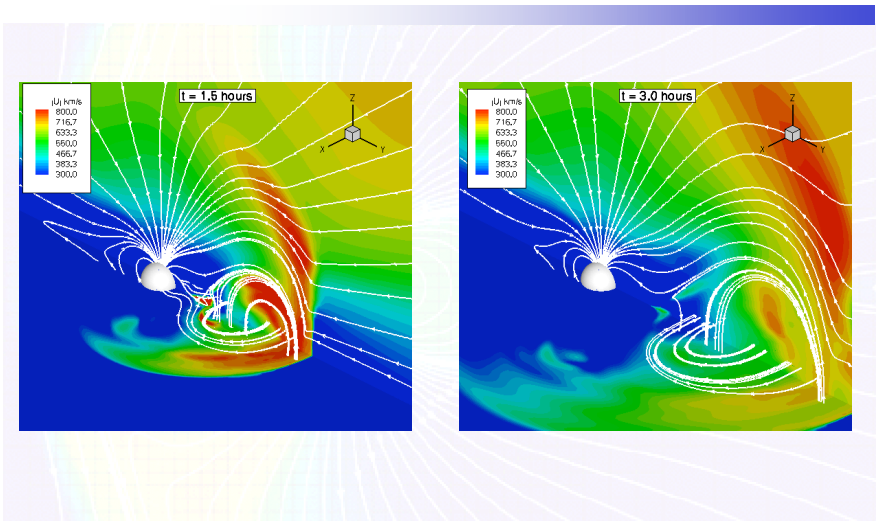

Grid Evolution

- AMR criterion: time derivative of density along Sun-Earth line tracks the shock
- Resolution 1/32 to 4 Rs
- 6X6X6 blocks
- 4.5 million to 14 million cells
- 4.5 days on 256 processors on O3K

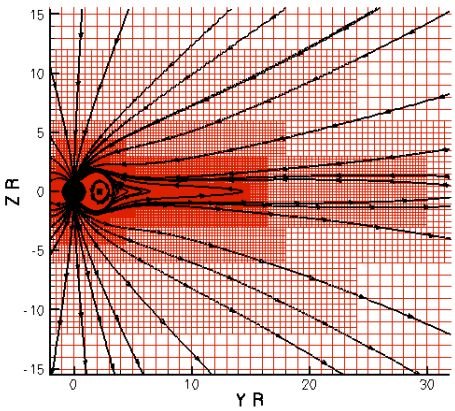

University of Michigan
Manchester et. al.
2003

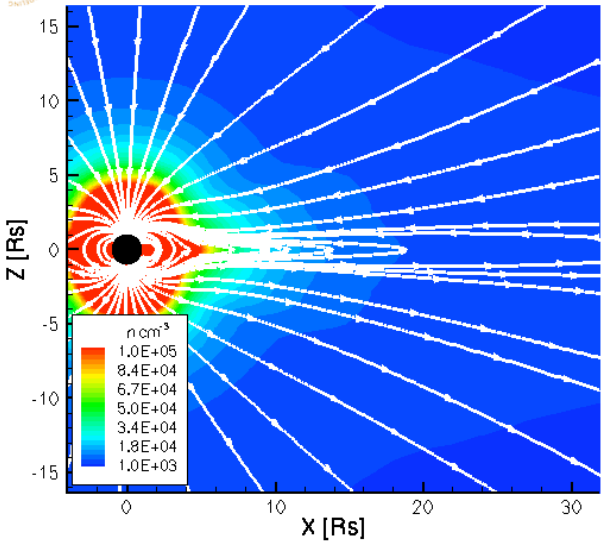

Flux Rope Driven CME Movie

- The movie shows the CME propagating outward.
- At 68.5 hours after initiation, when the leading edge reaches the Earth, the movie zooms in by a factor of 2000 and shows the interaction of the CME with the magnetosphere.

Pressure Pulse

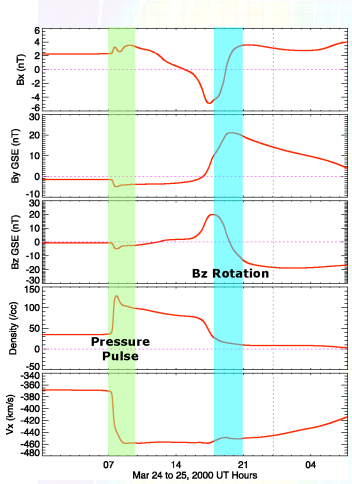

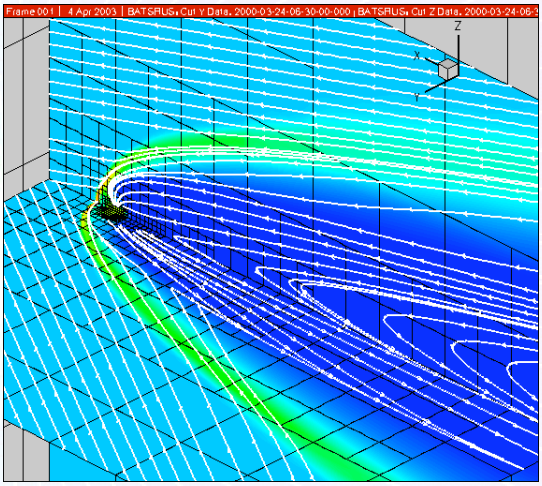

Center for Space Environment Modeling

http://csem.engin.umich.edu

Bz Rotation

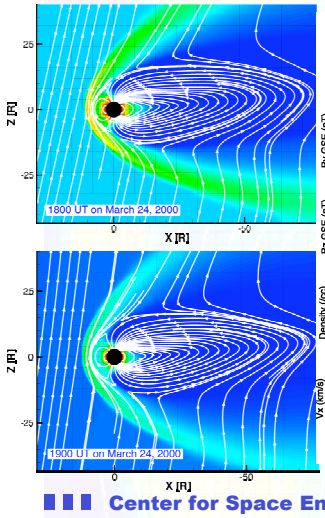

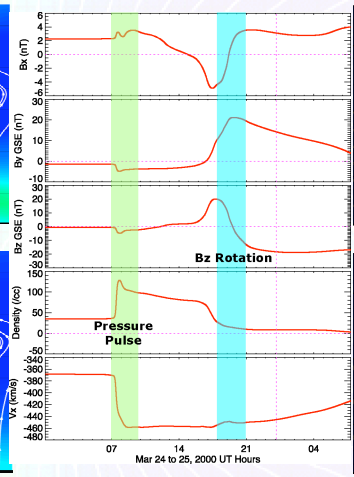

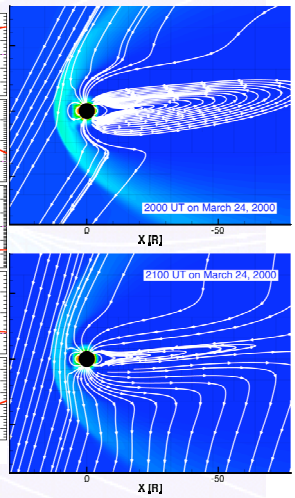

Center for Space Environment Modeling

http://csem.engin.umich.edu

Magnetogram Driven 3D Magnetic Field

Solar Wind Speed & Radial Magnetic Field at 1 AU

- Carrington map of the solar wind speed and radial magnetic field (contours) at R=1AU for the steady-state solar wind.
- The color code visualizes the solar wind speed in units of km/s. The position of the current sheet is shown by white dashed line.

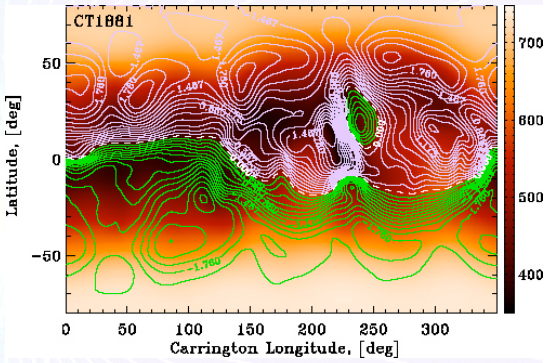

Center for Space Environment Modeling
http://csem.engin.umich.edu

3-D Close-up View of the Magnetic Topology

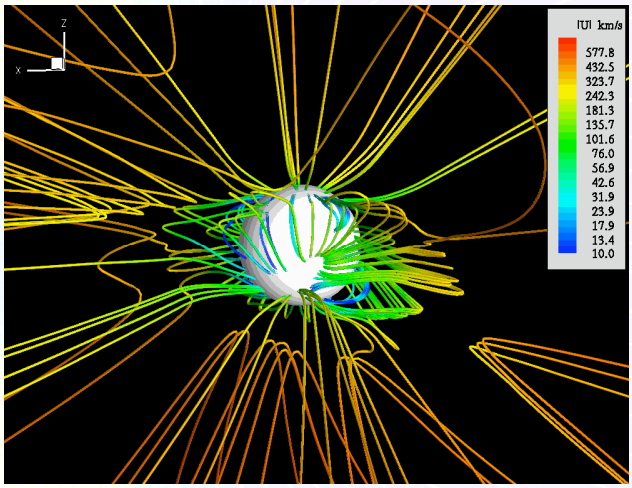

Magnetosphere for North/Southward IMF

Changing Magnetospheric Topology

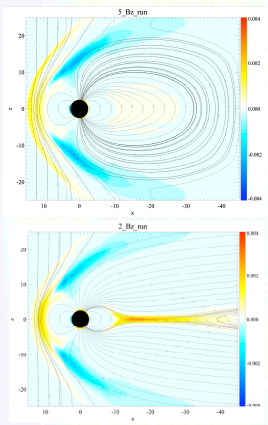

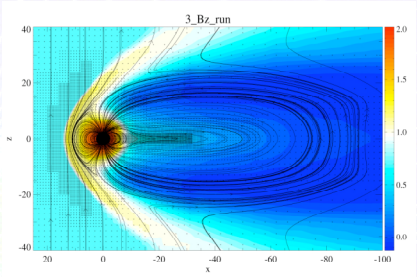

- The magnetospheric topology changes from "open" to "closed" at B_z~2.5 nT
- Recently Stauning (2002) found that NBZ FACs disappear around B_z~5 nT

Last Closed Field Lines for Northward IMF

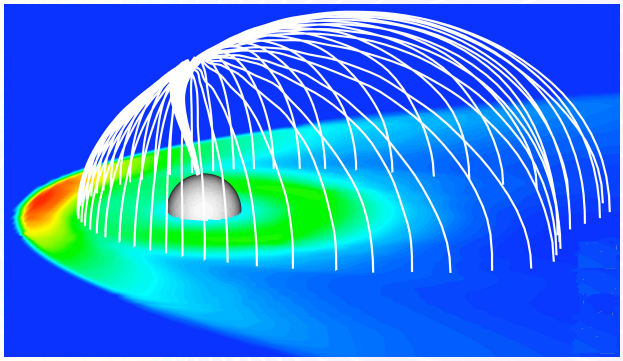

Magnetosphere for Northward IMF: Model and Simulation (Song et al., 1999)

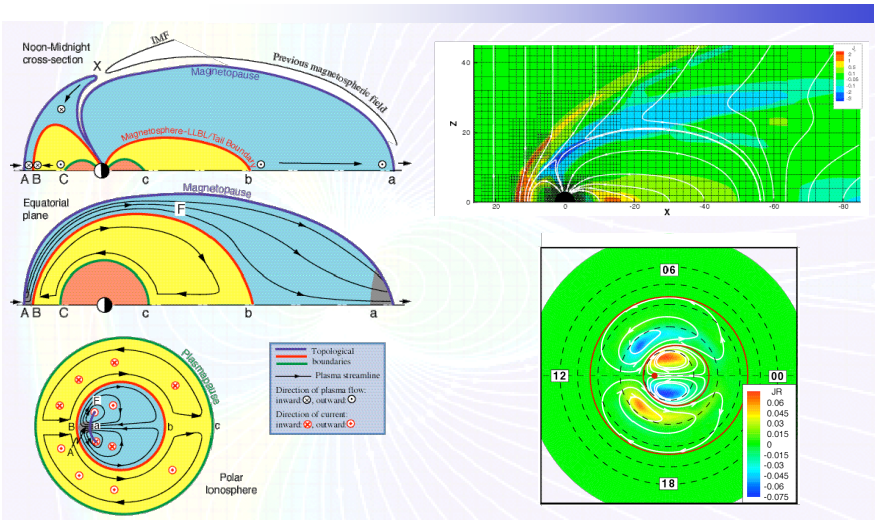

Center for Space Environment Modeling

http://csem.engin.umich.edu

Model Coupling

Center for Space Environment Modeling

http://csem.engin.umich.edu

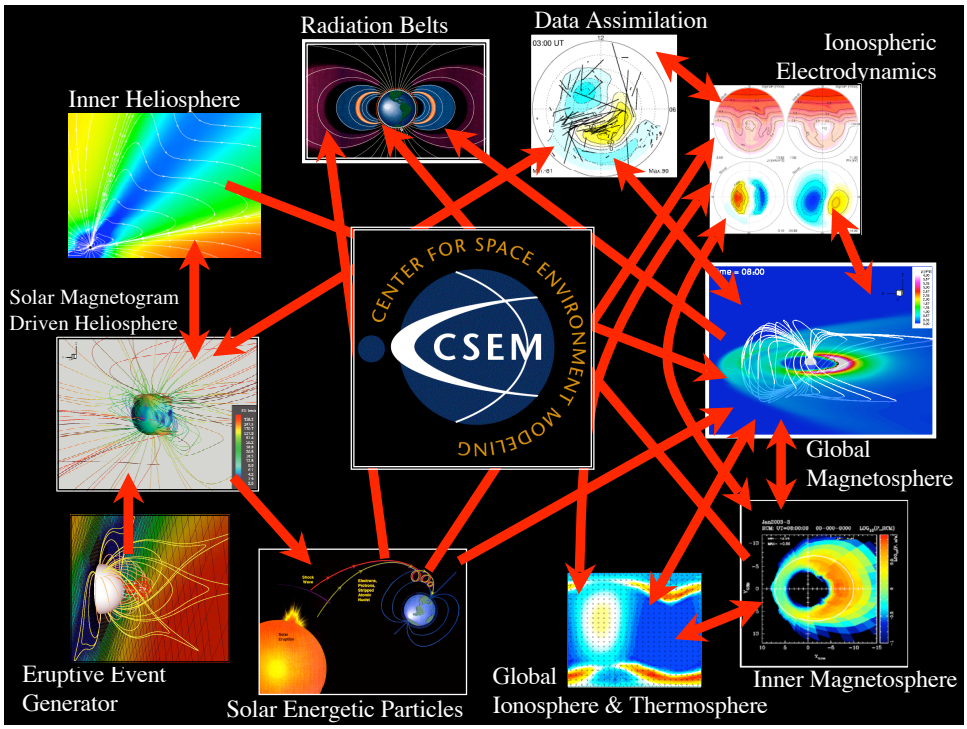

BATSRUS-Ionosphere Coupling
The Electrostatic Ionosphere

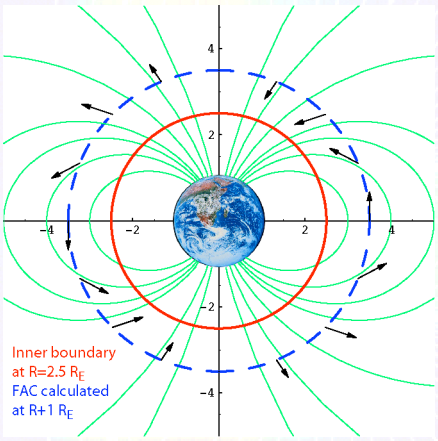

- $\mathbf{j}_{\parallel}$ is calculated from MHD near inner boundary.
- $\mathbf{j}_{\parallel}$ is projected along unperturbed dipole field lines into the height-integrated electrostatic ionosphere.
- $\mathbf{j}_t = \nabla_t \cdot (\Sigma \cdot \nabla \Phi)_t$ elliptic equation is solved for the ionospheric potential, Φ.
- Φ is projected back to the inner MHD boundary along unperturbed dipole field lines.
- Convection velocity is calculated at the inner boundary by $\mathbf{u} = (\mathbf{B}_0 \times \nabla \Phi) / B_0^2$ and it is used as inner boundary condition.

Center for Space Environment Modeling

http://csem.engin.umich.edu

BATSRUS–TIEGCM Coupling

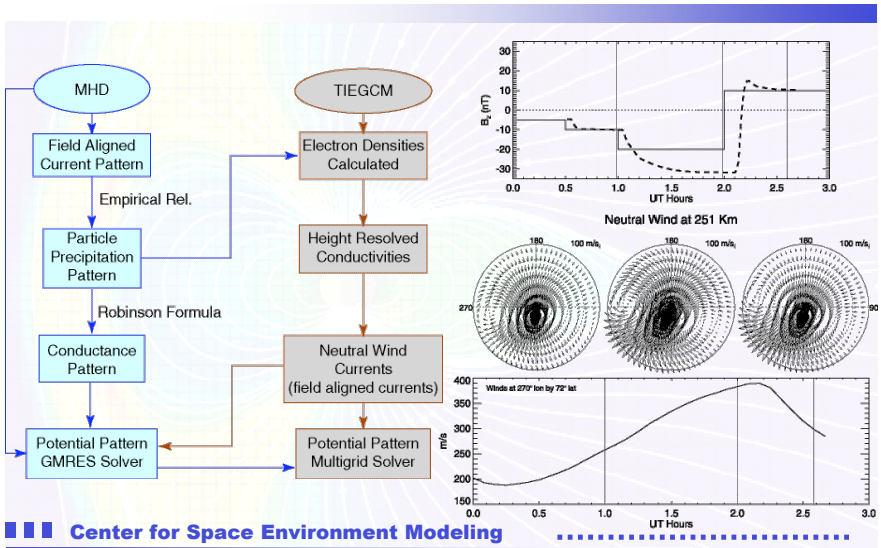

Center for Space Environment Modeling

http://csem.engin.umich.edu

BATSRUS–RCM Coupling

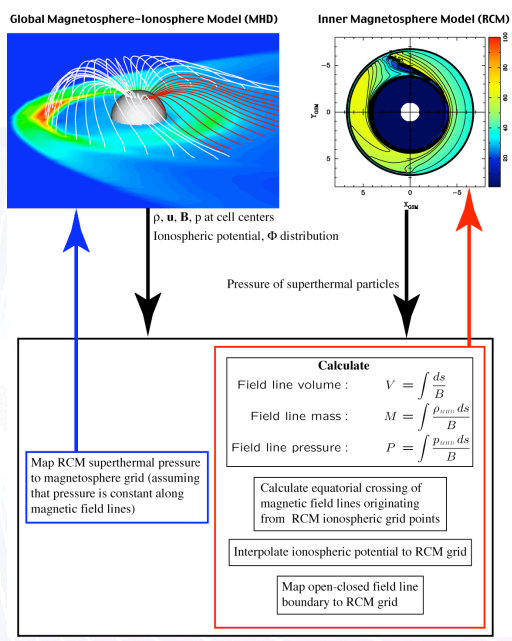

Center for Space Environment Modeling

http://csem.engin.umich.edu

Two Way Coupling between MHD and RCM

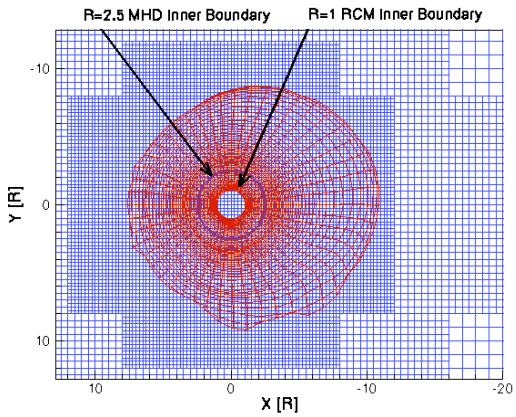

- The Pressure which is fed back to the MHD code by the RCM is used to drive the MHD pressure.
- The pressure is fed back on the RCM grid and is interpolated to the MHD grid
- Here we show the mapping at the initiation of the time accurate run.

Parallel Ray Tracing for BATSRUS-RCM Coupling

- Each block (black outlines) trace the field lines (white lines) contained in its block. The blocks then synchronize shared edges through a sequence of message passes until each trace is fully known.
- Time spent tracing is many thousands of times faster than serial tracing.
- Parallel efficiency improves with more processors and larger problems.

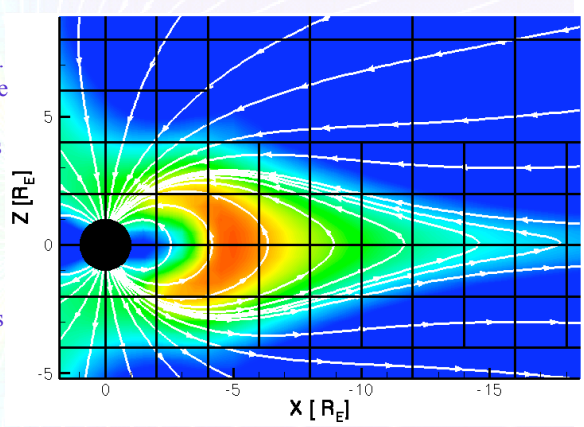

Time Accurate Coupled Run Description

- Standard steady solar wind conditions: Bz=-5nT
- At 8 hours, switch to Bz=+5nT at upstream boundary
- At 16 hours, switch back to Bz=-5nT
- Simple ionosphere: constant Pedersen conductance of 4S (Hall=0)
- Full MHD-RCM coupling every minute
- 854,016 computational cells (0.25 RE smallest) in the MHD simulation
- Serial RCM used 16% of computational time

Steady-State IMF South and North

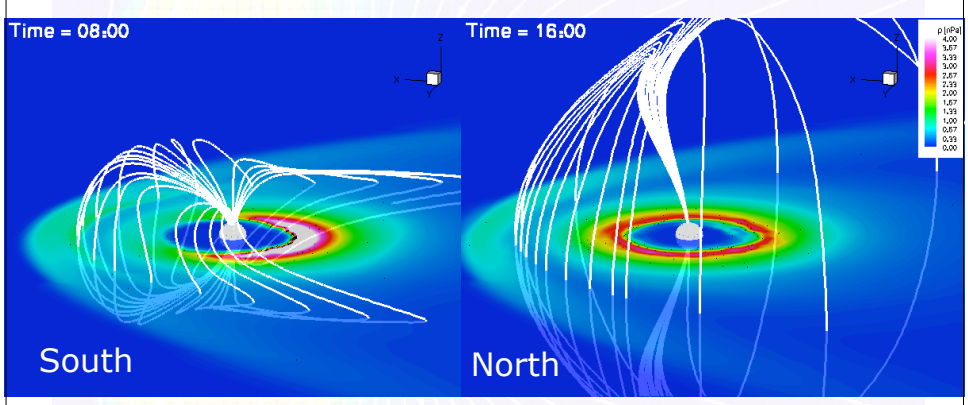

RCM Coupling: S-N-S Flip

The MHD-RCM coupling starts at t=0 with a steady IMF Bz=-5nT for 8 hours.

The partial ring current rapidly builds up and the neutral line moves from ~18 Re to ~30 Re.

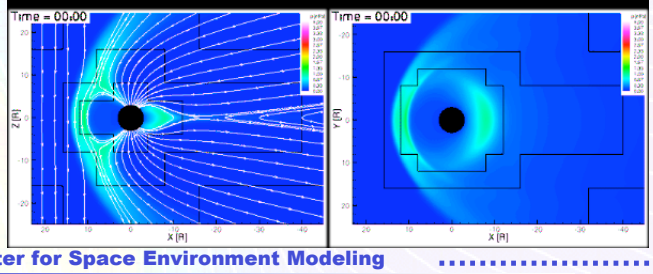

RCM Coupling: S-N-S Flip

At t=8 hours the IMF Bz flips from -5nT to +5nT.

The magnetosphere starts to change to Northward IMF configuration (closed tail).

The ring current becomes symmetric.

The ionosphere "fades" from Southward to Northward convection pattern.

Center for Space Environment Modeling
http://csem.engin.umich.edu

RCM Coupling: S-N-S Flip

In about 2 hours (t=10 h) the tail closes without releasing a plasmoid.

The steady Northward IMF conditions last until t=16 hours.

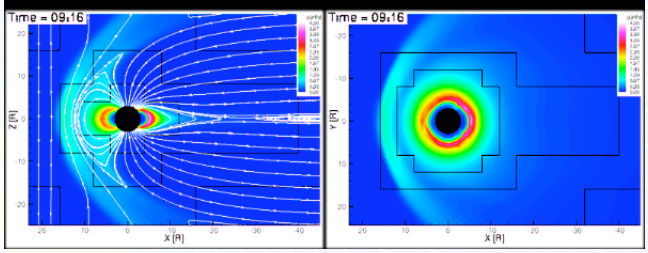

RCM Coupling: S-N-S Flip

At t=16 hours the IMF Bz flips from +5nT to -5nT.

The magnetosphere starts to change to Southward IMF configuration (open tail).

The ring current becomes asymmetric.

About an hour after the Bz flip a plasmoid is released.

The ionosphere "fades" from Northward to Southward convection pattern.

RCM Coupling: S-N-S Flip

By about t=19 hours the magnetosphere returned to the Southward configuration (3 hours after the Southward Bz flip).

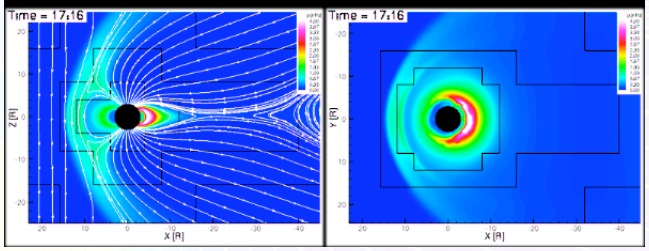

Center for Space Environment Modeling

http://csem.engin.umich.edu

IMF South to North Flip

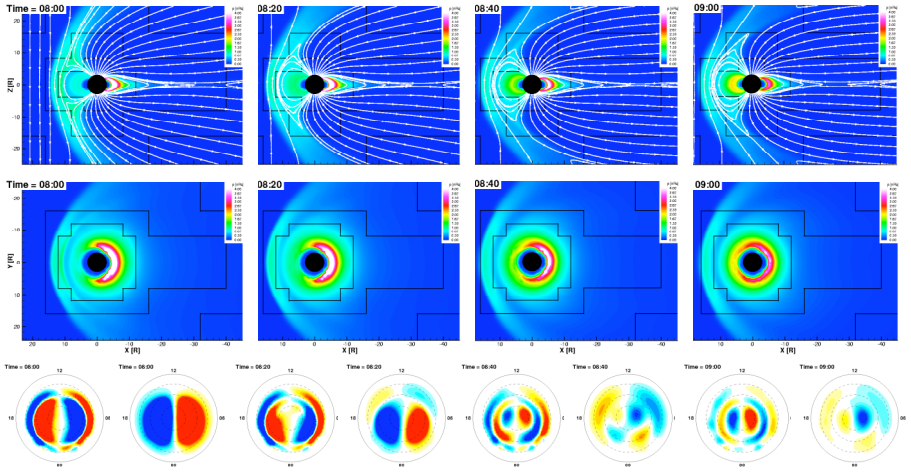

Center for Space Environment Modeling

http://csem.engin.umich.edu

Jupiter & Saturn Simulations

Center for Space Environment Modeling

http://csem.engin.umich.edu

Cassini's Jupiter Flyby

High ram pressure case

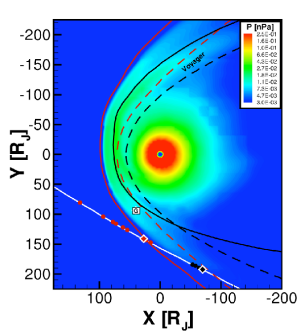

Low ram pressure case

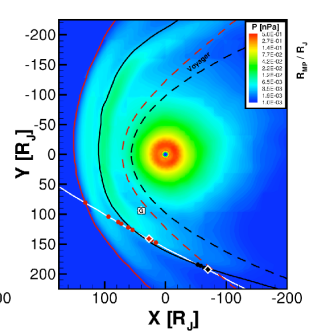

Comparison with the Huddleston et al. empirical magnetopause model

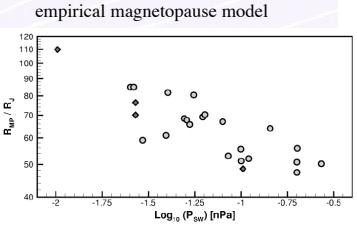

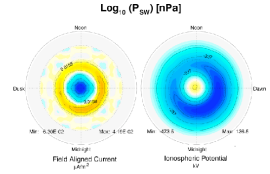

Coupled ionosphere simulation

Center for Space Environment Modeling

http://csem.engin.umich.edu

Io's Interaction with the Jovian Magnetosphere

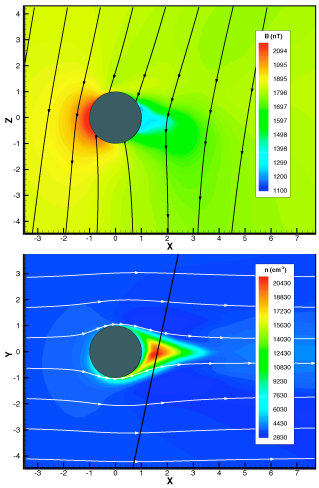

Galileo's first Io flyby in 1995

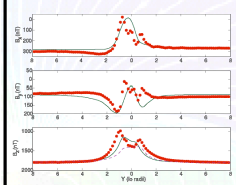

Kivelson et al., 1996

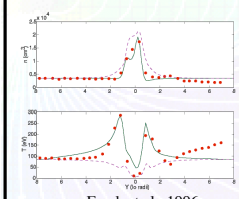

Frank et al., 1996

- No intrinsic magnetic field
- Two component atmosphere (exponential, power law)
- Lower boundary at surface
- Mass loading rate: 1.5×10^{28} s^{-1}
- Charge exchange rate: 2.3×10^{28} s^{-1}
- Reproduces Galileo observations reasonably well, but some physics is still missing

The Saturn-Titan System

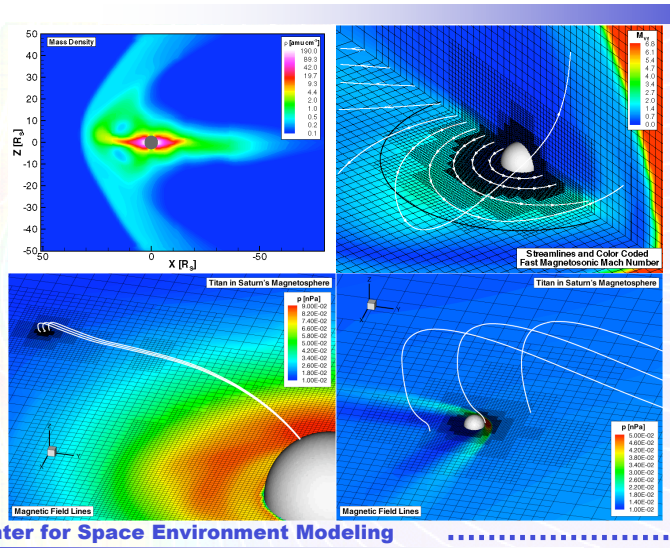

Terrestrial Planets

Mercury

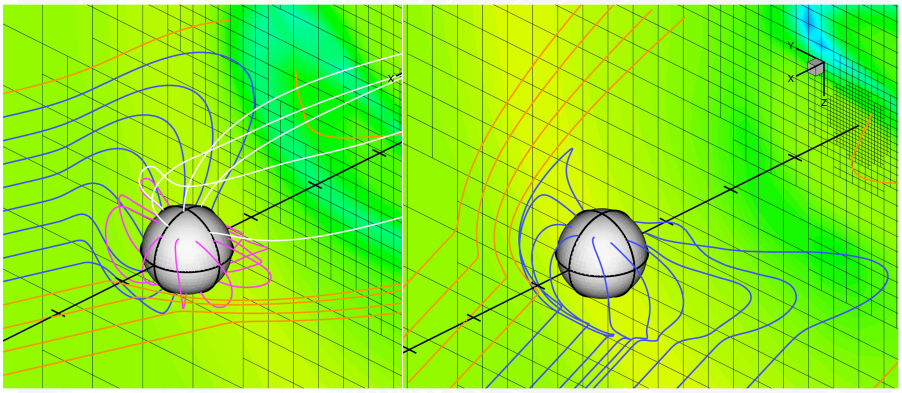

IMF South IMF North

Solar Wind Interaction with Venus

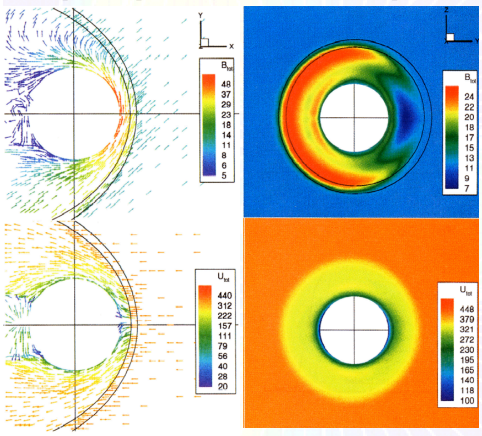

- Single species MHD with mass loading (cold and hot hydrogen and oxygen coronae)
- Charge exchange and ionization sources/sinks
- No intrinsic magnetic field
- IMF is 11 nT and is oriented 40° from the Sun-Venus line

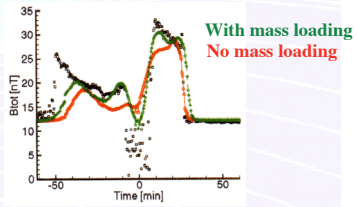

PVO Orbit 801

Solar Wind Interaction with Mars

- 3 Fluid AMR MHD model (H^+, O^+, O_2^+)
- Two cases:
  - Case 1: no intrinsic magnetic field
  - Case 2: Weak surface dipole (M= 2.6×10^{20} Gm^3) at 45°S latitude
- Results:
  - There is little difference in the global plasma environment between the two cases
  - The bow shock and ionopause locations are in good agreement with Phobos 2 observations
  - Heavy ion escape fluxes in the tail are in good agreement with Phobos 2 observations
  - Overall configuration is Venus-like

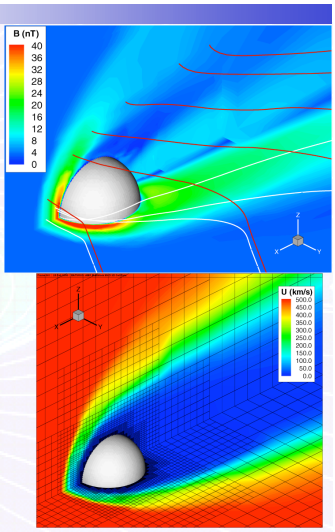

Mars Simulation with Crustal Fields

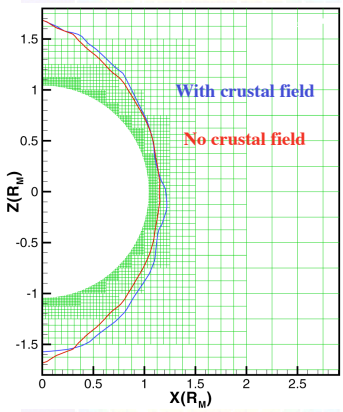

- 3 Fluid AMR MHD model (H^+, O^+, O_2^+)
- 60th-order harmonic expansion of the observed crustal magnetic field represents the intrinsic field of Mars
- Results:
  - Shock location is unaffected
  - Magnetopause/ionopause location modified
  - "Mini magnetocylinders" are formed by the crustal field
  - Transterminator and escape fluxes are consistent with Phobos-2 observations

	Observed Flux at Terminator	Calculated Flux at Terminator	Observed Escape Flux	Calculated Escape Flux
O^+	4.35×10^{25} s^{-1}	2.72×10^{25} s^{-1}	2.60×10^{25} s^{-1}	1.88×10^{25} s^{-1}
O_2^+	0.53×10^{25} s^{-1}	0.47×10^{25} s^{-1}	0.45×10^{25} s^{-1}	0.36×10^{25} s^{-1}
Total	4.88×10^{25} s^{-1}	3.19×10^{25} s^{-1}	3.05×10^{25} s^{-1}	2.24×10^{25} s^{-1}

Comets

Comet Halley Simulation

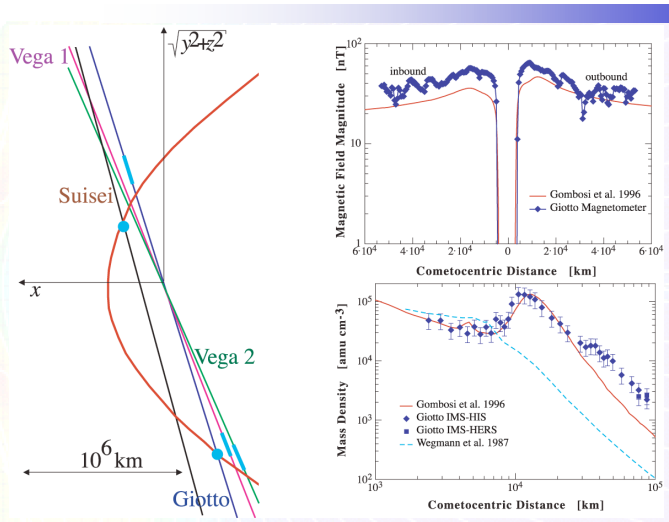

Center for Space Environment Modeling

http://csem.engin.umich.edu

Cometary X-Ray Simulation

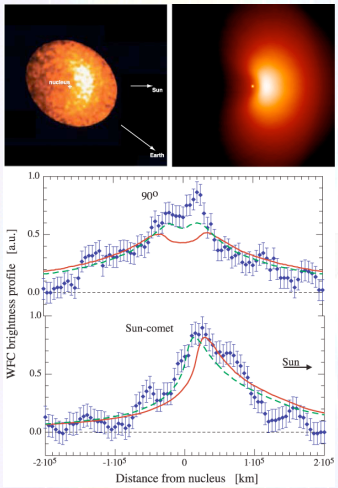

- ROSAT unexpectedly discovered x-ray emission from Hyakutake (Lisse et al., 1996).
- Cravens (1997) mechanism: x-ray emission is caused by charge exchange excitation of high charge state solar wind minor ions with cometary neutrals ($O^{7+} + H \rightarrow O^{6+*} + H^+$).
- X-ray emission was simulated using 14 solar wind minor ions (O^{7+}, O^{6+}, O^{5+}, O^{4+}, O^{3+}, C^{6+}, C^{5+}, C^{4+}, C^{3+}, Ne^{8+}, Ne^{7+}, Ne^{6+}, Ne^{5+}, Ne^{4+}).
- This process results in a line spectrum which primarily depends on the solar wind minor ion composition.
- Similar x-ray production is expected from planetary exospheres and from the outer heliosphere.

Center for Space Environment Modeling

http://csem.engin.umich.edu

Carrington Event (1859)

Carrington Event (1859)

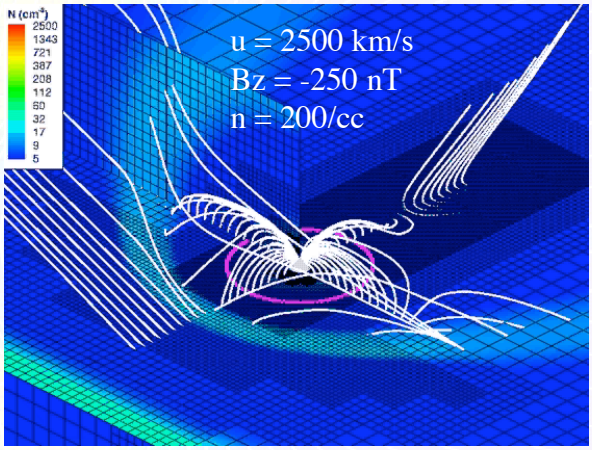

Carrington Event (1859)

Center for Space Environment Modeling

http://csem.engin.umich.edu